

Analysis of the hygroexpansion of a lignocellulosic fibrous material by digital correlation of images obtained by X-ray synchrotron microtomography: application to a folding box board

Jérémie Vigié · Pierre J. J. Dumont ·
Évelyne Mauret · Sabine Rolland du Roscoat ·
Pierre Vacher · Isabelle Desloges · Jean-François Bloch

Received: 2 December 2010 / Accepted: 9 February 2011 / Published online: 26 February 2011
© Springer Science+Business Media, LLC 2011

Abstract This study provides original experimental data on the microstructural mechanisms of the hygroexpansion of a material made up of lignocellulosic fibres. A paper-board made up of several layers was chosen and subjected to relative humidity variations during X-ray microtomography scanning. The 3D images of the evolving media were analysed using a digital image correlation technique to measure the displacement field within the studied material. This technique allowed the hygroexpansion of the studied material and of each layer of this latter to be analysed in the in-plane and out-of-plane directions. Results show that the hygroexpansion is highly anisotropic. The microstructural hygroexpansive mechanisms for the pore and fibre phases could also be revealed. They have been shown to depend strongly on the fibre content of the fibrous layers. This analysis provides also useful information concerning the

size of the Representative Elementary Volume (REV) for the hygroexpansion phenomenon of dense lignocellulosic fibrous networks. In view of the obtained results, the relevancy of common theoretical models used to predict the hygroexpansion of materials such as papers and boards is also discussed.

Introduction

The use of folding board as lightweight packaging material is growing in food, cosmetic and drug industries. Folding board is a fibrous stratified material. Each layer is made of pulps mainly composed of wood fibres and has an anisotropic structure due to the orientation of the fibres in the network, which results from the papermaking operations. Specific grades of pulps are chosen for layers depending on their location in the structure. Indeed, pulps differ in their extraction processes that can be either mechanical or chemical. To provide high (bending) stiffness and strength to the folding board structure, inner layers are often made up of low density mechanical pulps while chemical pulps are used for outer layers [1]. The folding board surface can be coated with pigments to improve the optical properties and printability.

Change in moisture content of folding board results in many deformation phenomena that can occur at different scales. Variations of moisture content can indeed induce hygroexpansion and curl at the laminate scale as well as they may lead to damage and delamination at the fibrous layer scale. These phenomena are associated with a significant loss of runnability during printing or converting operations.

Numerous authors studied these phenomena at the macroscopic scale by cycling the relative humidity of the

J. Vigié · P. J. J. Dumont (✉) · É. Mauret · I. Desloges ·
J.-F. Bloch
Laboratoire de Génie des Procédés Papetiers (LGP2), CNRS/
Institut Polytechnique de Grenoble (Grenoble INP), BP 65,
38402 Saint-Martin-d'Hères cedex, France
e-mail: pierre.dumont@grenoble-inp.fr

S. Rolland du Roscoat
Grenoble INP/UJF-Grenoble 1/CNRS, Laboratoire Sols-Solides-
Structures-Risques (3SR), BP 53, 38041 Grenoble cedex 9,
France

S. Rolland du Roscoat
European Synchrotron Radiation Facility (ESRF), ID 19
Topography and Microtomography Group, 38043 Grenoble
cedex, France

P. Vacher
Laboratoire SYMME, Université de Savoie, Polytech Savoie,
Domaine Universitaire, BP 80439, 74944 Annecy-le-Vieux,
France

air surrounding paper and board samples, which induces changes of the moisture content of paper. These experiments allowed them to reveal two typical features of the in-plane hygroexpansion with respect to the moisture content evolution. They observed a non linear hygroexpansion behaviour and irreversible deformation phenomena arising during the first cycles. Typically, shrinkage can be observed. Then, when increasing the number of cycles, reversible and linear hygroexpansion phenomena occur [2]. The slope of the curve of hygroexpansion as a function of the moisture content provides the hygroexpansion coefficient [3].

The in-plane hygroexpansion is influenced by the paper anisotropy (resulting from paper formation), by the pressing and mainly by the drying conditions. For instance, irreversible phenomena are usually related to the release of internal stresses initiated during the drying process [2]. These phenomena are particularly observed in restrained dried paper [3]. For reversible phenomena, it was shown experimentally that hygroexpansion coefficients are two to three times lower in the machine direction (MD) than in the cross direction (CD), depending on the sheet density [4]. The in-plane hygroexpansivity is two to four times higher in a freely dried paper than in a restrained dried paper [5]. In addition, the kind of pulp slightly affects the hygroexpansivity [6], and hygroexpansion can be significantly higher for pulps with high contents in fines [5].

There are fewer results for the *out-of-plane hygroexpansion* of paper [7–9]. Salmén and Fellers [9] have shown that the out-of-plane hygroexpansion coefficient can be ten times higher than the in-plane coefficients. They have also shown that for a freely dried paper the density has a strong influence on the hygroexpansion coefficient. This influence is lower for restrained dried paper. However, these papers exhibit a higher hygroexpansion coefficient than freely dried papers, in contrary to the in-plane phenomena.

Irreversible and reversible phenomena are noticed for curl similarly to the in-plane hygroexpansion. Curl is claimed to be related to heterogeneous distribution of the hygroexpansion properties of papers and boards through their thickness [10]. Curl can also occur when the moisture content of these materials is not uniformly distributed through the thickness [2].

The mechanisms of hygroexpansion and curl originate at the microscopic scale: i.e. the fibre scale. Indeed, the hygroexpansive behaviour of fibres is highly anisotropic. Their transverse hygroexpansion is one order of magnitude higher than their longitudinal one. At the mesoscopic scale: i.e. the fibrous network, Uesaka [4] identified the mechanism that governs hygroexpansion as a transfer of the hygroexpansive behaviour from the fibre to the fibrous network. This transfer is highly dependent on the configuration of the fibre–fibre bonding area. Concerning the

out-of-plane hygroexpansion, Salmén and Fellers [9] analysed theoretically the evolution of the pore volume when papers absorb moisture. This evolution depends both on paper density and drying conditions.

In order to measure the hygroexpansive strains of a paper sheet, several types of “expansimeters” were developed [2]. They consist in clamping a paper strip at both ends, one is fixed and the other is movable. Expansion or shrinkage of the sample causes the displacement of the movable end which is recorded. Lif et al. [11] used an electronic speckle photography system to study the in-plane strain field due to moisture absorption. The speckle pattern on the paper surface was produced by a spray-paint technique. Salmén and Fellers [9] assessed the out-of-plane hygroexpansion by thickness measurements. In the case of folding board, hygroexpansive strain measurements have been up to now limited to the macroscopic scale.

The objective of this article is to assess the actual hygroexpansive strain field in a folding board at the fibrous network scale. At this mesoscopic scale, the hygroexpansive strain field was measured by digital image correlation performed on images provided by X-ray synchrotron microtomography with in situ control of the relative humidity of the surrounding air. This technique, recently used to image papers [12, 13], gives access to the 3-D structure of samples in a non-destructive way. Besides, this technique allows the measurement of the variation of the fibre content through the board thickness during a moisture change. The final objective is to relate the hygroexpansive strain field to fibre content variations.

This study is organised as follows. The technical aspects related to the folding board structure, as well as to the experimental setups for moisture, hygroexpansion and curl measurements are given in the first section. The X-ray microtomography technique and the image correlation method are also detailed. Experimental results are presented in the second section. The hygroexpansive behaviour is investigated at the macroscopic and mesoscopic scales. Maps of the strain field of the folding board due to an increase of the moisture content are given. In the last section, the observed evolution is related to the fibre content of each layer. Finally, it is shown that the obtained results can be used to improve current approaches for modelling the hygroexpansion and curl of folding boards.

Materials and methods

Folding board

The studied folding board has a thickness e of 0.71 mm and a basis weight of 450 g m^{-2} . It is an assembly of 11 layers: three pigment layers and eight layers made up of virgin

pulps (mixture of hardwood and softwood fibres), formed on eight cylinder moulds. From its top face to its bottom face, the layers of the folding board are assembled as follows:

- two mineral pigment layers made up of calcium carbonate, kaolin and latex ($2 \times 10 \text{ g m}^{-2}$),
- two layers made up of bleached chemical pulp ($2 \times 30 \text{ g m}^{-2}$), named BCP1,
- one layer made up of bleached mechanical pulp (60 g m^{-2}), named BMP1,
- three layers made up of mechanical pulp ($3 \times 60 \text{ g m}^{-2}$), named MP,
- one layer made up of bleached mechanical pulp (60 g m^{-2}), named BMP2,
- one layer made up of bleached chemical pulp (30 g m^{-2}), named BCP2,
- one mineral pigment layer similar to the previous ones (10 g m^{-2}).

It can be noticed that mechanical pulp is associated with production “brokes”, i.e. reslushed boxboard, (until 40% in weight). Moreover, a slurry of cooked starch was sprayed between mechanical and chemical layers to improve bonding (between 7 and 10 g m^{-2}). This folding board was supplied by Cascades Group (La Rochette, France).

Isotropic laboratory papers

The pulps of the folding board layers were used to produce isotropic laboratory paper sheets using a Rapid Köthen former (Karl Frank GMBH, Weinheim, Germany). The basis weights of the sheets were chosen to be in accordance with those of the folding board layers. A conventional pressing stage was carried out for all the papers. As it was not possible to know the actual drying conditions for the folding board layers, two sets of sheets were prepared. Some were freely dried and the others were dried under constraint (or restraint). Cross sections of each sheet were imaged using an Environmental Scanning Electron Microscope (ESEM), Quanta 200 from FEI (Eindhoven, The Netherlands), at a relative humidity of 20%. Then, the average thicknesses of the sheets were measured. Finally, the average densities of freely dried and restraint-dried sheets were calculated. Results are shown in Table 1. For

the sake of simplicity, the names of the laboratory papers are those of the corresponding layers of the folding board. These data will be used to perform structural analysis in the next section. It can be observed that the average densities of sheets are slightly higher for restraint-dried sheets than for freely dried sheets for all tested pulps. Nonetheless, the dispersion of these results remain quite large, which does not permit to conclude definitely on the structural differences induced by both types of drying conditions on the basis of this simple measurement of apparent densities. These data will be used for the identification of the layers of the folding board in Sect. [Layer identification](#).

Moisture, hygroexpansion and curl measurement setups

The moisture content evolution of the folding board was measured at $23 \text{ }^\circ\text{C}$ with the especially designed Varimass[®] device (Techpap, Grenoble, France) for five relative humidity steps: $50 \rightarrow 20 \rightarrow 80 \rightarrow 20 \rightarrow 50\%$. Each step lasted for 4 h, except for the first one, which was limited to 2 h. Hygroexpansive strains associated to the same relative humidity steps were recorded with the Varidim[®] device (Techpap, Grenoble, France). These systems include a wet air generator, with a compressed air pretreatment device and a control unit, a test chamber where the samples are placed and a computer that allows the entire process control with two software applications. The air generator provides the test chamber with conditioned air. The controlled relative humidity ranges from 15 ± 2 to $90 \pm 2\%$.

In the Varimass[®] system, the mass of a sample m_s is recorded using a precision balance with an accuracy of $\pm 0.5 \text{ mg}$. Then, the moisture content c is calculated using the mass of the dry sample m_{sdry} (oven dried for 24 h at $105 \text{ }^\circ\text{C}$) as follows:

$$c = \frac{m_s - m_{\text{sdry}}}{m_{\text{sdry}}} \quad (1)$$

The Varidim[®] system allows the length variation of ten samples of 15 mm in width and 150 mm in length to be measured. The samples are vertically fastened with magnetic clamps at both extremities, and the bottom clamp is movable and attached to a LVDT displacement sensor. The accuracy of the measurement reaches $\pm 3 \text{ } \mu\text{m}$. The hygroexpansive strain ε_h can be calculated as:

Table 1 Apparent densities of freely dried and constraint dried isotropic laboratory papers (kg m^{-3})

	BCP1	BMP1	MP1	MP2	MP3	BMP2	BCP2
Freely dried	720 ± 10	580 ± 10	550 ± 20	550 ± 20	550 ± 20	580 ± 10	720 ± 10
Constraint dried	725 ± 10	590 ± 10	570 ± 20	570 ± 20	570 ± 20	590 ± 10	725 ± 10

$$\epsilon_h = \frac{\Delta L}{L_0}, \tag{2}$$

where L_0 is the length at the end of the first relative humidity step at 50% RH, and ΔL is the length variation. Tested samples were cut along the CD and MD of the folding board. At the end of each step, the moisture content and the hygroexpansive strain tend to stabilise: samples has reached an equilibrium configuration.

Curl of the folding board was characterized by measuring the curvature of five samples of 15 mm in width and 150 mm in length in a test chamber provided with conditioned air at 23 °C. Three steps of relative humidity were chosen: 50 → 20 → 50 % RH. The strips, cut in the CD and MD, were centrally supported in a standing position along their long edges by pins. Curvatures were assessed using a millimetre paper placed underneath. A similar method has been developed for curl measurements of wood–fibre mats [14].

Image acquisition by X-ray microtomography

All images shown in this study were acquired at the European Synchrotron Radiation Facility (ESRF) in Grenoble, France. During data acquisition, a parallel and monochromatic X-ray beam irradiates the sample. Radiographs of the X-ray beam (20.5 keV) passing through the sample are recorded for different angular positions (1500) between 0° and 180°. According to the typical size of the fibrous constituents of paperboard, a voxel size of $0.7 \times 0.7 \times 0.7 \mu\text{m}^3$ was chosen, giving an imaged volume of $1400 \times 1400 \times e \mu\text{m}^3$, i.e. $2048 \times 2048 \times e/0.7$ voxels. A filtered back-projection algorithm is applied to reconstruct the 3D structure of the sample using the scanned radiographs. When performing absorption-based X-ray microtomography, the reconstructed 3D volume represents a 3D map of the coefficient of absorption of the sample

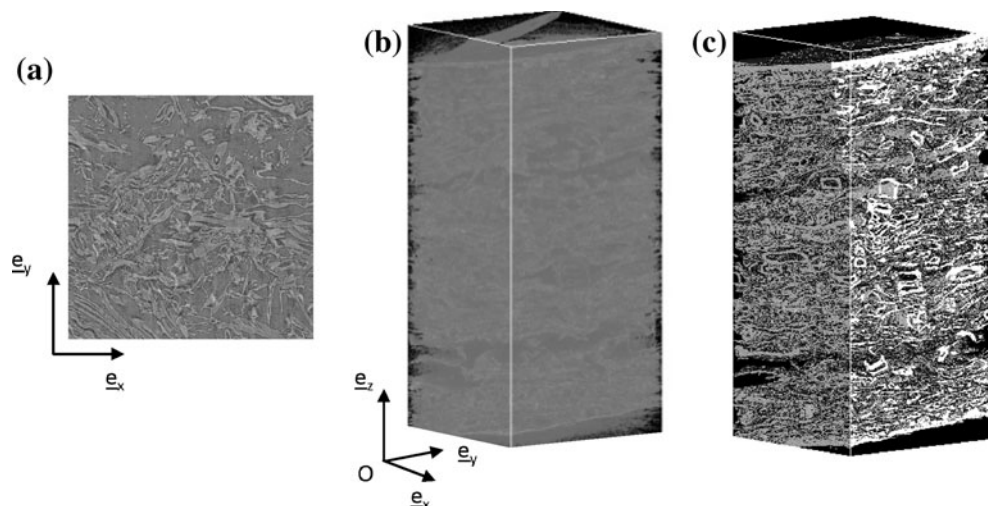
constituents. The values of the absorption coefficients are represented as different values of grey level coded in 32 bits. Figure 1b reveals a small volume extracted from the whole imaged volume of $500 \times 500 \times 1024$ voxels. Figure 1a depicts a plane cross section of this volume. In order to obtain quantitative descriptors of the sample structure, image treatment operations were performed. These operations consist in segmenting the image to distinguish the porous and fibrous phases. This was performed using segmentation algorithms developed by Rolland du Roscoat et al. [12] for the analysis of paper imaged by X-ray microtomography. The obtained segmented volume is depicted in Fig. 1c. It should be noticed here that it was checked that the directions \underline{e}_x and \underline{e}_y pretty much correspond respectively to the MD and to the CD of the folding board despite the slight tilt of the sample (less than 5° around the \underline{e}_x -direction).

In this study, the relative humidity of the air surrounding the sample was in situ controlled during the image acquisition. The sample first stabilised at 50% RH, afterwards two relative humidity steps were performed: 20 → 50%. The duration (~20 min) of each step was chosen so as to reach an equilibrium configuration of the sample. The air with controlled relative humidity was delivered to the analysed sample using a similar wet air generator as those used in the Varimass® and Varidim® systems. The macroscopic hygroexpansive strain ϵ_{ZD} of the sample was calculated as the ratio of the thickness variation Δe for the jump of relative humidity between 20 and 50% RH to the reference thickness e of the sample measured at 20% RH (see Fig. 2).

Digital image correlation technique

In order to study the hygroexpansive behaviour of the folding board, a 2D Digital Image Correlation (DIC)

Fig. 1 **a** Cross section of the imaged volume of a 450 g m^{-2} folding board made up of virgin pulps at 20% RH extracted at $z = e/2$. **b** Imaged volume. **c** Imaged volume after the segmentation operation. In images **a** and **b** fibres appear as light grey. Pores appear as dark grey. In the segmented image **c**, fibres are in white and pores in black



technique was used. This technique relies on comparing the pattern matching of two grey intensity images coded in 32 bits obtained before and after a relative humidity change. This comparison allows the measurement of the relative displacement of the points of the two images. These images were extracted from the 3D microtomographic volume of $500 \times 500 \times 1024$ voxels (see Fig. 1b). Indeed, such images of the sample exhibit a random grey intensity distribution, which can be used as a random speckle pattern. Images extracted from the volume reconstructed at 20% RH were used as reference images and compared with images extracted from the volume scanned at the final step of 50% RH. In the reference image, some cross sections parallel with the $(\underline{e}_x, \underline{e}_z)$ and $(\underline{e}_y, \underline{e}_z)$ planes in the middle of the volume were cut, as shown in Fig. 2.

In this study, the DIC software 7D[®] [15] was used. The principle of this software is to divide a reference image into small interrogation windows having a size of 30×30 pixels. Then, the displacement of the summits of small interrogation windows is tracked in the final image using a correlation technique. For this purpose, a subset of 30×30 pixels centred around the summits of the interrogation windows is defined. A normalised cross correlation criterion is used to find similarities between subsets of the initial image and pixel zones of the final image. In order to calculate this criterion, it is necessary to interpolate the grey level variations in the reference and final images. Here, a bilinear interpolation function for the grey level was used for both images. Then, knowing the displacements of the four summits of the interrogation window, the

displacement field in this window is interpolated using again a bilinear interpolation function. As the shape of the subsets of pixels may evolve between the reference and final images, their detection needs an iterative process. This latter involves to use at each step the updated displacement of the summits of the interrogation windows. The error on the displacement measurement obtained with this method can be evaluated equal to 0.2 pixel. This corresponds to an error of $0.14 \mu\text{m}$ in the studied images.

Of course, when using a 2D image correlation technique for measuring displacements in microtomographic images, one difficulty consists in finding the images of the final configuration to be analysed. In this study, several cross sections were extracted from the volume of the final configuration (at 50% RH) parallel with the $(\underline{e}_x, \underline{e}_z)$ and $(\underline{e}_y, \underline{e}_z)$ planes as in the case of the reference image 2. The DIC technique was used to determine for each chosen initial cross section the best corresponding cross section of the final image. It appeared that whatever the initial cross section we tested, there was always one single final plane giving an optimal correlation. In that case, the number of the interrogation windows which were found was always higher than 80%. This percentage corresponds to a good correlation because it accounts for porous zones where the correlation cannot work and regions with poor contrast over the top and below the bottom of the sample, see Figs. 1c and 2. It was then possible to obtain the local displacement field $\underline{u}_1 = u\underline{e}_x + w\underline{e}_z$ in the plane $(\underline{e}_x, \underline{e}_z)$ and the local displacement field $\underline{u}_2 = v\underline{e}_y + w\underline{e}_z$ in the plane $(\underline{e}_y, \underline{e}_z)$. Figure 3a shows the w component of the local displacement field \underline{u}_1 given by the 7D[®] software. Complete maps of this field were built using the Matlab[®] software (function Griddata), as depicted in Fig. 3b for the w component. This allowed the small strain tensor $\underline{\varepsilon} = 1/2(\underline{\text{gradu}} + {}^t\underline{\text{gradu}})$ to be assessed numerically by a centred finite difference scheme.

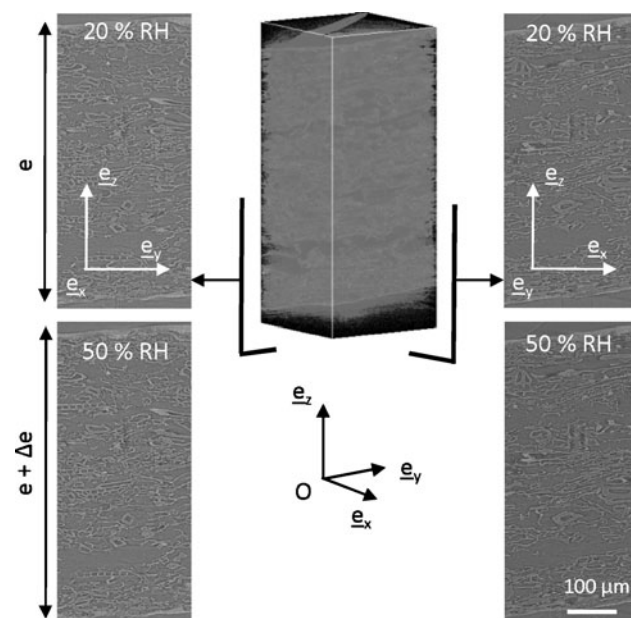


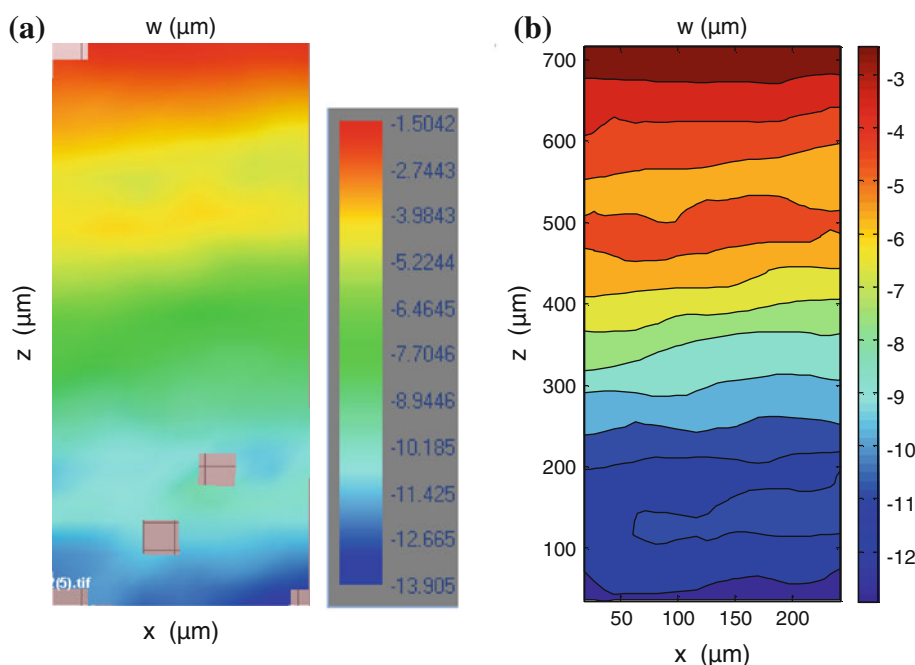
Fig. 2 Cross sections cut in the middle of the reconstructed volumes parallel with planes $(\underline{e}_x, \underline{e}_z)$ and $(\underline{e}_y, \underline{e}_z)$ at 20 and 50% RH

Results

Hygroexpansive behaviour at the macroscopic scale

Figure 4a depicts the evolution of hygroexpansive strains in the MD and CD at the end of each step with respect to the moisture content. In the CD, the hygroexpansive strain is -0.28% at the lowest moisture content, whereas it reaches 0.38% at the highest moisture content. In the MD, the strains are respectively -0.14 and 0.06% . The variation between the lowest and highest values of moisture content was assumed to be linear for both tested directions. This permitted to calculate the slopes of these curves and then

Fig. 3 **a** Map of the measured w component of the displacement field in the plane ($\mathbf{e}_x, \mathbf{e}_z$) obtained with 7D[®] software. **b** Same map built by Matlab[®] software



the in-plane coefficient of hygroexpansion of the folding board along the MD and CD β_{MD} and β_{CD} , respectively (see Fig. 4a). The hygroexpansion coefficient in the CD is almost three times greater than that in the MD, revealing thus a strong anisotropic behaviour.

The hygroexpansive strain in thickness direction noted ϵ_{ZD} is represented with respect to the moisture content at two humidity steps 20 and 50% RH in Fig. 4b. As expected, the hygroexpansive strain in the thickness direction is largely higher than the values measured in plane. The out-of-plane hygroexpansion coefficient β_{ZD} is four times greater than the CD one. This result is in accordance with the values obtained by Salmén and Fellers [9].

Table 2 gives the curvatures of the folding board measured along the MD and CD, respectively κ_{MD} and κ_{CD} . At the end of the first step at 50% RH, the folding board samples are perfectly flat. At 20% RH, the curvature

measured along the MD is positive. This means that the centre of curvature of the folding board is located in the \mathbf{e}_z positive direction. Along the CD, the curvature is negative, i.e. the centre of curvature of the folding board is located in the \mathbf{e}_z negative direction. Similarly to what is observed for the in-plane hygroexpansion, the curvature is four times greater in the CD than in the MD. At the end of the final step of 50% RH, curvatures reached again very low values.

Hygroexpansive behaviour at the mesoscopic scale

The hygroexpansive behaviour at the mesoscopic scale was studied using the DIC and the microtomographic images as it has been previously explained. Due to the fact that displacements were measured exclusively in the planes ($\mathbf{e}_x, \mathbf{e}_z$) and ($\mathbf{e}_y, \mathbf{e}_z$), only the components $\epsilon_{xx}, \epsilon_{yy}, \epsilon_{zz}, 2\epsilon_{xz}$

Fig. 4 **a** Evolution of the hygroexpansive strains ϵ_h in the MD and in the CD with respect to moisture content measured by the Varimass[®] and Varidim[®] devices. **b** Evolution of the hygroexpansive strain ϵ_{ZD} in thickness direction measured in microtomographic images

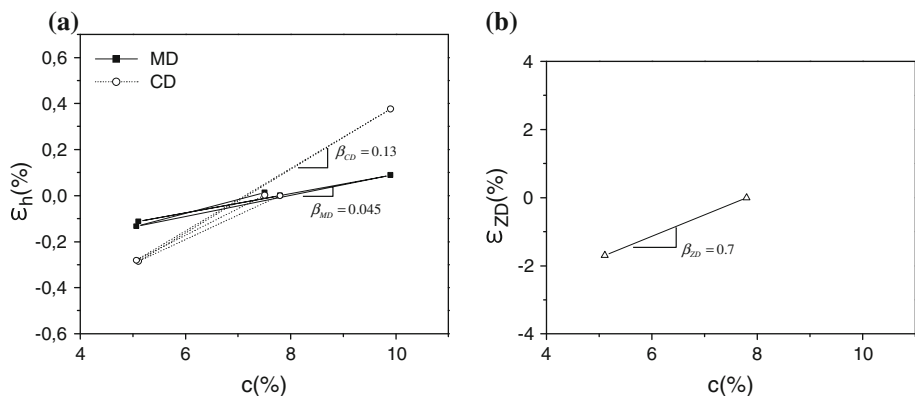


Table 2 Curvatures of folding board samples in the machine direction κ_{MD} and in the cross direction κ_{CD} at different relative humidities

	50% RH (ref)	20% RH	50% RH
κ_{MD} (m^{-1})	0	0.30 (± 0.05)	0
κ_{CD} (m^{-1})	0	-1.5 (± 0.1)	-0.1

and $2\varepsilon_{yz}$ of the small strain tensor could be calculated. These components are given by

$$\begin{aligned} \varepsilon_{xx} &= \frac{\partial u}{\partial x}, \quad \varepsilon_{yy} = \frac{\partial v}{\partial y}, \quad \varepsilon_{zz} = \frac{\partial w}{\partial z} \\ 2\varepsilon_{xz} &= \frac{\partial u}{\partial z} + \frac{\partial w}{\partial x}, \quad 2\varepsilon_{yz} = \frac{\partial v}{\partial z} + \frac{\partial w}{\partial y} \end{aligned} \quad (3)$$

These calculations were performed for three parallel cross sections of the studied sample. Similar results could be obtained whatever the studied cross sections. Thus, in the following, results of a pair of two perpendicular representative cross sections are presented. Figure 5 shows maps of the strain components related to a relative humidity change from 20 to 50% RH. As the w component could be measured in both perpendicular representative studied cross sections, the component ε_{zz} of the strain field could be

provided twice. It could be checked that the strain values in the intersection line (see the dashed line in Fig. 5) of the two perpendicular studied planes are similar. It should be noticed here that the hygroexpansive strain components were not calculated in the outer folding board layers which are composed of mineral pigments. These layers exhibit very uniform grey levels. Therefore, the DIC cannot distinguish any pattern and does not permit to follow the displacement field of these particular layers.

As shown in Fig. 5, the components of the hygroexpansive strain field are largely heterogeneous. The in-plane components ε_{xx} and ε_{yy} show juxtaposed areas with positive and negative values. This reveals a complex deformation phenomenon at the scale of the fibre network. Unfortunately, these maps do not allow a precise description of the hygroexpansion phenomena at the fibre scale. This point would necessitate further investigations. The behaviour of the ε_{zz} component is different. It varies a lot through the thickness of the sample but remains relatively homogeneous at a given z coordinate (see Fig. 5). Thus, it appears that the hygroexpansive behaviour of the folding board is particularly influenced by its layered structure. In order to analyse precisely this phenomenon, the average strain

Fig. 5 Maps of the components of the hygroexpansive strain field related to a relative humidity change from 20 to 50% RH, calculated using the displacement field measured in two perpendicular planes extracted in the middle of a volume imaged by X-ray microtomography (450 g m^{-2} folding board made up of virgin pulps). The dashed line represents the intersection line of the two studied planes. $\langle\langle \varepsilon_{xx} \rangle\rangle$ and $\langle\langle \varepsilon_{yy} \rangle\rangle$ denote here the average values of the strain components calculated over the surface of the tested planes. $\langle\langle \varepsilon_{zz} \rangle\rangle$ is calculated similarly except that both tested planes are considered

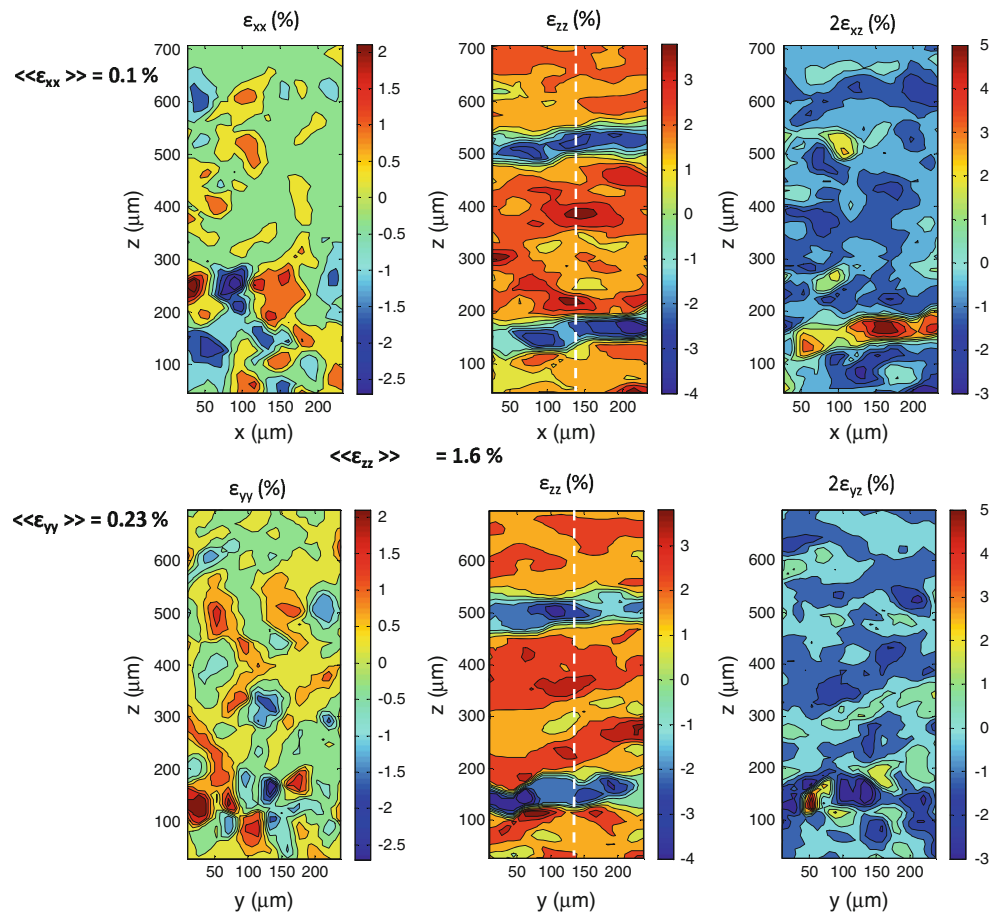
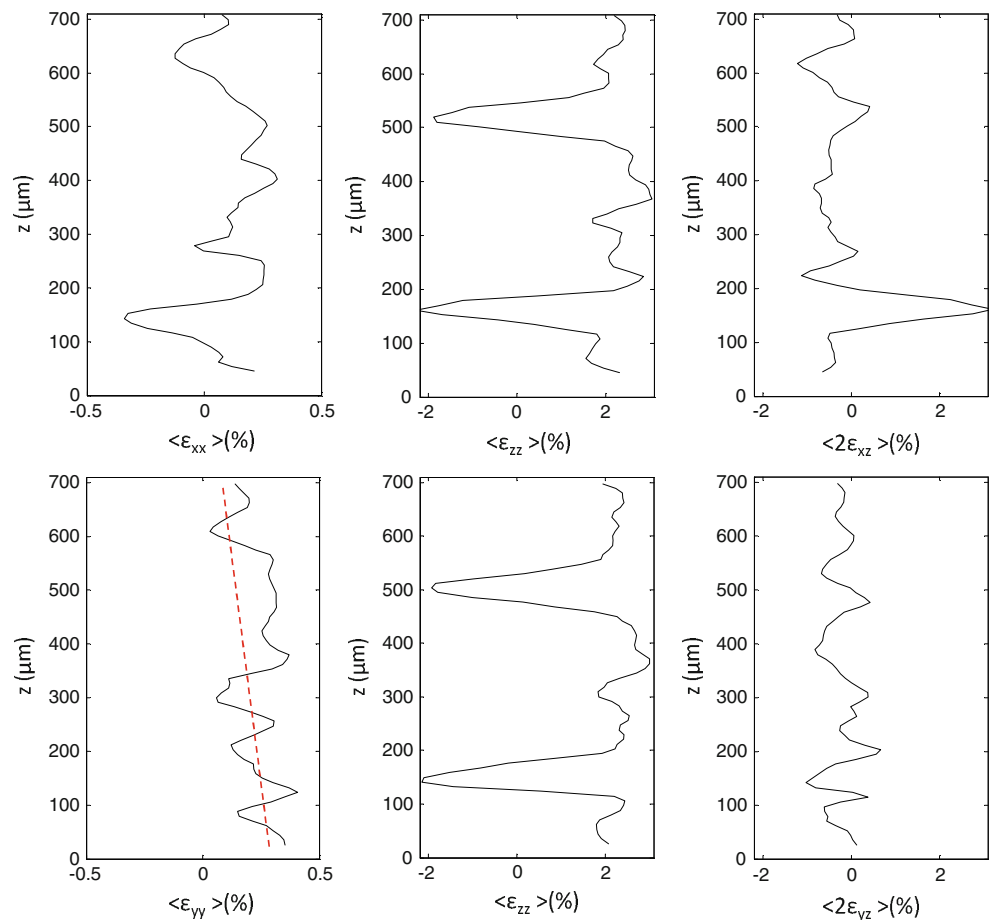


Fig. 6 Profiles in the thickness direction of the average value of the components of the hydroexpansive strain tensor. The *dashed line* represents a linear fit of $\langle \varepsilon_{yy} \rangle$



profiles in the thickness are plotted in Fig. 6. These profiles depict a large heterogeneity in the thickness direction for all the strain components. The component ε_{xx} varies from -0.3 to 0.3% , ε_{yy} from 0.1 to 0.4% and ε_{zz} from -2 to 3% . Furthermore, it has to be noticed that the average transverse shear components of the strain tensor $2\varepsilon_{xz}$ and $2\varepsilon_{yz}$ reach higher values than those of the in-plane components, as depicted in Figs. 5 and 6.

Fibre content profiles through the thickness

Figure 7 shows the profiles of the fibre content through the thickness of the folding board in the previously considered cross sections parallel with $(\underline{e}_y, \underline{e}_z)$. One profile f_0 was obtained at 20% RH and the other one f_1 at 50% RH. These profiles are found to be highly heterogeneous. For both profiles, the fibre content varies from 10 to 70%. Two regions have a high porosity. They can be easily identified in the microtomographic volume (see Fig. 1). It is worth noting that the evolution of f_1 slightly differs from the evolution of f_0 in some regions of the thickness.

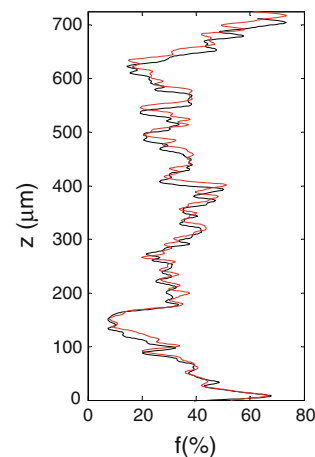


Fig. 7 Profile f_0 of fibre content at 20% RH (black line) and profile f_1 at 50% RH (grey/red line) (Color figure online)

Discussion

Layer identification

The thickness of each layer was determined considering the following procedure. First, three regions through the

thickness of the folding board were identified. These regions are separated by two highly porous zones which clearly appear in the microtomographic volume (see Fig. 1c). They correspond to the minimum value of the ε_{zz} component reached on the profiles as shown in Fig. 6. It was assumed that these characteristic zones could correspond to the interfaces between the bleached and unbleached mechanical layers because of their poor adhesive properties since no starch paste was added between them. This allows a bottom region to be defined. This region was assumed to contain the so called layers BCP2 and BMP2. A middle region can also be defined. This one contains the three layers of unbleached mechanical pulp, which are designated by MP. The top region is composed of BMP1 and BCP1. Then, it was assumed that the relative thickness of each layer in each region could be determined from the densities of the laboratory papers produced using the various pulps of the folding board (see Table 1). For that purpose, the densities measured for freely dried and restraint-dried conditions were averaged. Finally, in order to consider the interfacial zones between the three regions, 15 μm was added to the thickness of each neighbouring layer BMP1, MP1, MP3 and BMP2.

Thereafter, the average value of the strain $\langle\langle\varepsilon_{zzk}\rangle\rangle$ of each layer k could be calculated as it is illustrated in Fig. 8a for the plane $(\mathbf{e}_y, \mathbf{e}_z)$ in the thickness direction. Layers made up of chemical pulp show almost the same hydro-expansive strains, around 2%. On the contrary, layers made up of mechanical pulp depict largely heterogeneous behaviours: average strains vary from 1.2 to 2.4%. Figure 8b specifies the average value $\langle f_0 \rangle$ of fibre content at 20% RH for each layer. As expected, the fibre content is higher in layers made up of chemical pulp than in layers made up of mechanical pulp. This is an effect of the

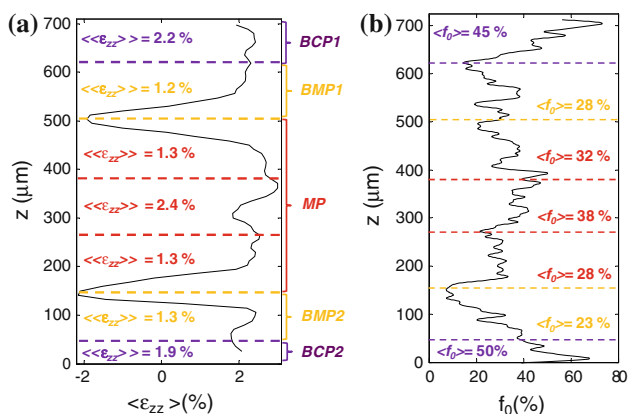


Fig. 8 **a** Profile of the average value $\langle\varepsilon_{zz}\rangle$ in the thickness direction in the plane $(\mathbf{e}_y, \mathbf{e}_z)$ and related average values $\langle\langle\varepsilon_{zz}\rangle\rangle$ for each layer. **b** Profile of the fibre content through the paperboard thickness and average value of the fibre content $\langle f_0 \rangle$ of each paperboard layer at 20% RH

well-known lower compressibility of mechanical pulps compared with chemical pulps [17]. This effect can also be observed with the laboratory papers (*cf.* Table 1).

Relations between the hydroexpansive strain and the structure evolution

The evolution of the average hydroexpansive strain in the thickness direction $\langle\langle\varepsilon_{zz}\rangle\rangle$ with respect to the average fibre content $\langle f_0 \rangle$ is shown in Fig. 9a. The layers with the highest fibre contents ($\geq 38\%$; notice that this value is an ad hoc value due to the layers forming the specific tested folding board) exhibit the highest hydroexpansive strains, ranging between 1.9 and 2.2%. All these layers are made up of chemical pulps except for the layer MP2, which also exhibits an average hydroexpansive strain slightly higher than those recorded for the chemical pulp layers. For fibre contents below 38%, it can be observed that the hydroexpansive strain is only equal to 1.2–1.3%, i.e. merely constant. All these layers which have low fibre contents are made up of mechanical pulps.

Is it the fibre content or the type of pulps which have the primary influence on the hydroexpansion in the thickness

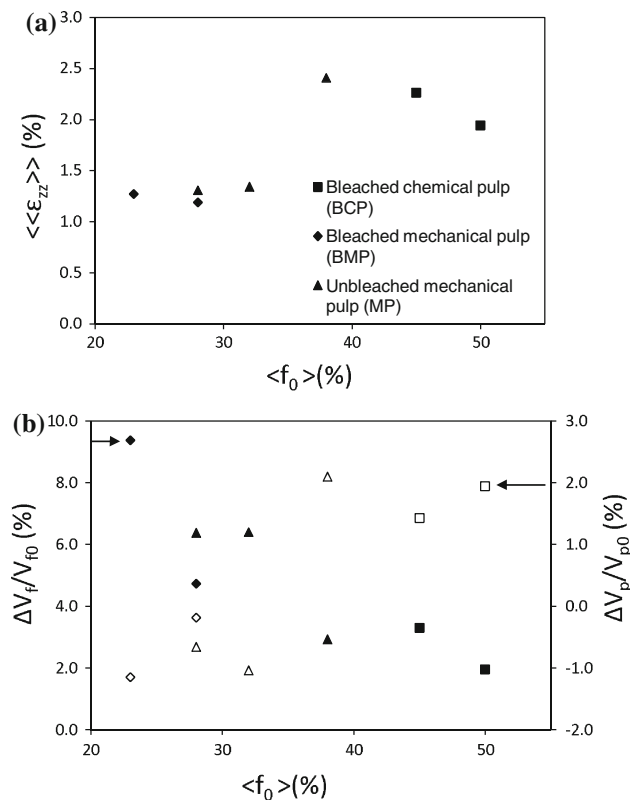


Fig. 9 **a** Evolution of the average hydroexpansive strain in the paperboard thickness $\langle\langle\varepsilon_{zz}\rangle\rangle$ with respect to the fibre content $\langle f_0 \rangle$. **b** Relative variations of pore (open symbols) and fibre (black symbols) phases (with respect to the fibre content $\langle f_0 \rangle$)

direction? This question is difficult to answer using only the set of data gained here. It is all the more difficult to give a definite answer as it may be assumed for instance that the high hygroexpansive behaviour of the MP2 layer could be attributed both to the high fine content of mechanical pulps, which is known to increase the hygroexpansive strain [5, 6], or to a possible high content in chemical pulp fibres from the reslushed brokes (see Sect. **Materials and methods**). This latter assumption is nevertheless improbable as the layers MP1 and MP3 which contain the same type of pulps as MP2 should certainly show similar hygroexpansive behaviour as MP2.

The fibre fraction and the type of pulps parameters have certainly both a great influence on the hygroexpansion phenomenon. Notice that drying conditions should also be taken into account as a third influential parameter. The present observations open as perspectives to test the hygroexpansive behaviour of layers made up of mechanical pulps which would have higher fibre contents than those of the tested industrial folding board. Conversely, the behaviour of chemical pulp layers with low fibre contents should also be investigated.

In order to better understand the dependence between the hygroexpansive behaviour and the structural properties of the investigated folding board, the evolution of the volumes of the pore and fibre phases was estimated.

As shown in the previous sections, the average value $\langle\langle \epsilon_{zz} \rangle\rangle$ is largely greater than the average values $\langle\langle \epsilon_{xx} \rangle\rangle, \langle\langle \epsilon_{yy} \rangle\rangle$. Consequently, the relative volume variation of the sample can be calculated as follows:

$$\frac{V_1 - V_0}{V_0} = Tr(\underline{\underline{\epsilon}}) \approx \langle\langle \epsilon_{zz} \rangle\rangle, \tag{4}$$

where V_0 and V_1 are the volumes of the sample at 20% RH and 50% RH, respectively and $Tr()$ is the trace operator. It is further assumed that the relative variation of the volumes of porous and fibrous phases can be estimated using a mixture law:

$$\begin{aligned} \langle\langle \epsilon_{zz} \rangle\rangle &\approx \frac{V_{f1} - V_{f0}}{V_{f0}} \langle f_0 \rangle + \frac{V_{p1} - V_{p0}}{V_{p0}} (1 - \langle f_0 \rangle) \\ &= \frac{\Delta V_f}{V_{f0}} \langle f_0 \rangle + \frac{\Delta V_p}{V_{p0}} (1 - \langle f_0 \rangle), \end{aligned} \tag{5}$$

where V_{f0} and V_{p0} are the initial volumes of fibrous and porous phases, respectively, V_{f1} and V_{p1} are the final volumes. V_{f0} and V_{p1} were estimated considering the total volume of each layer and their fibre content (using data of Figs. 7 and 8).

Figure 9b exhibits the variation of $\Delta V_f/V_{f0}$ and $\Delta V_p/V_{p0}$ with respect to the average fibre content at 20% RH $\langle f_0 \rangle$ for each layer. As expected, the volume of the fibre phase always increases when the relative humidity varies from 20% RH to 50% RH, which corresponds to a moisture

content increase. Moreover, the variation of the volume of the fibre phase is highly pronounced for layers with low fibre contents ($<38\%$). This is a sign that fibres are mainly not strongly constrained to deform in this situation. Nevertheless, the out-of-plane hygroexpansive strains of these layers remain low. This observation could be explained by a mechanism where the high fibre expansion is compensated by a large decrease of the pore volume (see Fig. 9b and Table 3). This particular behaviour certainly requires that the hygroexpansion of fibres is heterogeneous: fibres could be constrained from swelling at regions of inter-fibre bonding; whereas segments of fibres between bonded areas would be “free” to swell. This mechanism should be confirmed by further experimental observations. By contrast, the swelling of fibres is weak in the densest layers ($\geq 38\%$): the density of bonded areas is higher in this situation so that fibres are certainly more homogeneously constrained from swelling through their bonded areas. However, the overall hygroexpansion is larger than for low density networks because there is apparently no compensation of fibre expansion by pore volume decrease.

This is also very interesting to focus on the hygroexpansion behaviour of the layers by considering their pore volume variation. It can indeed be observed that the pore volume slightly decreases in layers with fibre contents lower than 38%; whereas it increases in layers with higher fibre content. However, whatever the considered layers, the gain remains lower than the gain of the fibre volume, except for the highest fibre content (the gains of pore and fibre volumes are equal for the layer BCP2, see also Table 3). In this latter case, this observation means that the porosity of the BCP2 layer remains the same between both studied states. In all other less dense layers, the porosity decreases with the moisture increase. This effect is here again particularly visible for fibrous networks with the lowest fibre contents ($<38\%$) where the decrease of porosity is combined with a decrease of the pore volume. For denser layers ($\geq 38\%$), the decrease of porosity occurs as well but is combined with a pore volume increase. This means that the pores, even if they can expand, can be seen in all cases as partially “filled” due to the more important fibre swelling during the fibrous network expansion. For the densest layers, this phenomenon is not flagrant because

Table 3 Density of each layer (kg m^{-3}) of the studied folding board using the average fibre content determined from microtomographic images, corresponding strain in the thickness direction and relative pore volume variation

	BCP1	BMP1	MP1	MP2	MP3	BMP2	BCP2
Density (kg m^{-3})	675	420	480	570	420	345	750
$\langle\langle \epsilon_{zz} \rangle\rangle$ (%)	2.2	1.2	1.3	2.4	1.3	1.3	1.9
$\Delta V_p/V_{p0}$ (%)	1.4	-0.2	-1.1	2.1	-0.7	-1.2	1.9

the variation of the pore volume shows a tendency to follow the overall expansion of the layers and the fibre volume variation (see also Fig. 9b and Table 3).

Salmén and Fellers [9] studied the hygroexpansion mechanisms of freely dried papers and restrained dried papers with respect to their density. Based on various assumptions, they could relate the hygroexpansion mechanisms of papers to expansion mechanisms of their pore and fibre phases. They have observed that the hygroexpansion coefficient of freely dried papers in the thickness direction increases with their density. For the highest paper densities, this coefficient reaches values close to those observed for papers dried under restraint, i.e. the kind of papers which exhibit the highest hygroexpansivity in the thickness direction. They have also shown that the hygroexpansion of freely dried papers having densities lower than 500 kg m^{-3} is accompanied by a pore volume which is unchanged or slightly decreases for a relative humidity jump between 40 and 65% RH. Furthermore, they have observed that the hygroexpansion of the same type of papers with densities higher than 500 kg m^{-3} is related to a pore volume increase. This mechanism is all the more pronounced as the density of papers is higher. For the highest density values, the variations of the pore and fibre phase volumes are close.

For comparison, we have reported in Table 3 the density of each layer of the studied folding board, estimated from the average fibre content and the cellulose density ($\approx 1500 \text{ kg m}^{-3}$), as well as the corresponding strain and the relative variation of the pore volume. One can note that the densities slightly differ from those given in Table 1 for layers BMP1, BMP2, MP1 and MP3 because of the interfacial zones between the three regions previously identified. These data show also that the hygroexpansive behaviour of the low density layers ($<500 \text{ kg m}^{-3}$) of the studied folding board (BMP1, BMP2, MP1 and MP3) follows the same tendencies for both the influence of the density and the relative pore volume variations as those observed by Salmén and Fellers for freely dried papers. It is also possible to notice a clear analogy between the behaviour of the densest layers ($>500 \text{ kg m}^{-3}$) of the studied folding board (BCP1, MP2 and BCP2) and the observations of Salmén and Fellers.

Nonetheless, it is not possible to conclude definitely e.g. about the drying conditions the layers of the folding board were subjected to. Indeed, as previously reported, Salmén and Fellers [9] have noticed that the hygroexpansive behaviour in the thickness direction of freely dried and constraint-dried papers is quite similar when their density is high. Thus, further experiments should be performed on a similar material to the studied board with various and controlled drying conditions.

What representative elementary volume for the hygroexpansive behaviour of folding board?

One current issue of the microstructure characterisation by microtomography is the determination of the minimum size of the sample to be scanned to perform an experiment which delivers a representative description (or response) of the material for a considered microstructural property (or physical phenomenon). This consists in determining the Representative Elementary Volume (REV). The REV is a priori not unique and may depend on the studied property or phenomenon. Regarding the microstructural properties, e.g. the porosity, it was shown for a large number of papers that an imaged volume of $1400 \mu\text{m} \times 1400 \mu\text{m} \times$ thickness can be considered as being larger than the minimum size required for a volume to be representative [13]. It was also shown in [18] that volumes of similar sizes give representative results for the effective permeability and thermal conductivity of these materials. Here, we can provide some insights into the hygroexpansive behaviour of the tested folding board. The average values of the components ε_{xx} , ε_{yy} and ε_{zz} could be calculated by integrating the data of the maps of Fig. 5. They reached 0.1, 0.23 and 1.6% respectively. These values were used to estimate the hygroexpansion coefficients in the MD and CD that were compared with those measured using the macroscopic measurement technique. Results are shown in the Table 4. It is worth noting that the obtained values are in the same order of magnitude and that the ratios between the hygroexpansion coefficients in the MD and CD are close. Although the values measured at the macroscopic scale are greater, the set of studied planes seems to be reasonably representative of the hygroexpansive behaviour of the macroscopic structure.

The determination of the REV can also be theoretically supported. As previously mentioned in the introduction, the hygroexpansive behaviour of the fibre network is thought to be mainly controlled by the configuration of fibre–fibre bonding zones. Le Corre et al. [19] estimated, in the framework of a tube model approach [20], the average number \bar{Z} of fibre–fibre contacts per fibre, also called the coordination number, for planar network of straight

Table 4 Hygroexpansion coefficients in the MD and CD of the folding board assessed at the macroscopic and mesoscopic scales

	β_{MD}	β_{CD}
Macroscopic value	0.045	0.13
DIC value	0.036	0.098
Difference (%)	21	24

cylindrical fibres with an elliptical cross section, the major and minor axes of which are d_{\max} and d_{\min} , respectively. This number is expressed as follows

$$\bar{Z} = n_f l \delta^* (l d_{\min} \Phi_1 + d_{\max} d_{\min} \Phi_2 + d_{\max} d_{\min}), \tag{6}$$

where n_f is the number of fibres per unit volume, l the length of the fibres, δ^* a dimensionless parameter which governs the size of a control volume, Φ_1 and Φ_2 are 2D-orientation functions. Here, this model was used to roughly estimate the number of inter-fibre bonds per fibre in layers made up of mechanical and chemical pulps. It has to be noticed that this model is based on a “soft core” approach: i.e. fibres are considered as cylinders that may overlap and interpenetrate. Other models such as in Batchelor et al. [21] which are based on a “hard core” approach where the fibre flexibility is included could also be used. It can be checked that this soft core approach gives a reasonable estimate of the number of fibre–fibre contacts per fibre compared with the previously cited hard core approach and even with experimental measurements [22].

The parameter n_f was calculated using the fibre volume fraction $\langle f_0 \rangle$ measured previously and considering that wood fibres were straight with an elliptical cross section, δ^* had to be chosen equal to 2 for directly contacting fibres, $\Phi_1 = 2/\pi$ and $\Phi_2 = 2/\pi$ considering a planar isotropic orientation of fibres. The length l , the width d_{\max} and the thickness d_{\min} of the fibres of the mechanical and chemical pulps were estimated from experimental measurements performed using a specially designed apparatus (Morfi, Techpap, Grenoble, France) and scanning electron microscopy. All these dimensions are given in Table 5. They are typical of those observed in paper materials [23]. For mechanical pulp fibres, \bar{Z} can be estimated ranging between 6 to 10, whereas it ranges between 40 to 44 for chemical pulp fibres. This means that the distance between the centre of adjacent inter-fibre bonds is of the order of 50 μm for the mechanical pulp layers, whereas it is of the order of 30 μm for the chemical pulp layers. This is in agreement with the estimation given by Alava and Niskanen [24]. Then, the length of the scanned volume is about 28 to 47 times greater than the inter-fibre bond distance, i.e. the characteristic length of the microstructural heterogeneity for the hygroexpansion phenomenon. According to this estimation, the hygroexpansive behaviour of the

imaged volume, despite its small dimensions, is representative of the paperboard behaviour.

Thereafter, we wondered whether the folding board curvatures could be predicted from the in-plane strain profiles through thickness (see Fig. 6) using classically modelling approaches. Up to now, approaches for the curl prediction are based on plate theories [25, 26, 27,28]. These theories assume the form of the displacement field [29]. Various displacement formulations can be used to consider only in-plane components of the strain field (classical theory) or transverse shear (first-order and third-order shear theories). In these approaches, the in-plane components of the displacement field vary linearly with the thickness coordinate z . For instance, in the first-order shear theory, the displacement components are written as follows:

$$\begin{aligned} u(x, y, z) &= u_0(x, y) + z\phi_x(x, y) \\ v(x, y, z) &= v_0(x, y) + z\phi_y(x, y) \\ w(x, y, z) &= w_0(x, y) \end{aligned} \tag{7}$$

where $\phi_x(x, y)$ and $\phi_y(x, y)$ denote the rotations of a transverse normal about the y -axis and the x -axis, respectively.

As a consequence, the in-plane components of the strain field ϵ_{xx} , ϵ_{yy} and $2\epsilon_{xy}$ are linear through the laminate thickness, while the transverse shear components $2\epsilon_{xz}$ and $2\epsilon_{yz}$ are constant and ϵ_{zz} is zero [29]. Then, the strain tensor components can be written using a vector notation as follows:

$$\begin{Bmatrix} \epsilon_{xx} \\ \epsilon_{yy} \\ 2\epsilon_{xy} \\ 2\epsilon_{xz} \\ 2\epsilon_{yz} \end{Bmatrix} = \begin{Bmatrix} \epsilon_{xx}^{(0)} \\ \epsilon_{yy}^{(0)} \\ 2\epsilon_{xy}^{(0)} \\ 2\epsilon_{xz}^{(0)} \\ 2\epsilon_{yz}^{(0)} \end{Bmatrix} + z \begin{Bmatrix} \epsilon_{xx}^{(1)} \\ \epsilon_{yy}^{(1)} \\ 2\epsilon_{xy}^{(1)} \\ 0 \\ 0 \end{Bmatrix} \tag{8}$$

where $\epsilon_{xx}^{(0)}$, $\epsilon_{yy}^{(0)}$, $2\epsilon_{xy}^{(0)}$, $2\epsilon_{xz}^{(0)}$ and $2\epsilon_{yz}^{(0)}$ are the mid-plane strains and $\epsilon_{xx}^{(1)}$, $\epsilon_{yy}^{(1)}$ and $2\epsilon_{xy}^{(1)}$ are defined as the curvatures of the plate. Obviously, such formulation of the displacement and of the strain fields involves large simplifications compared with the observed fields by DIC (see Figs. 5 and 6). Furthermore, such theories neglect the most significant component ϵ_{zz} of the hygroexpansive strain field.

In spite of this point, this is nevertheless interesting to investigate whether the assumption of linearity through the thickness of the in-plane components of the strain tensor holds. Here, the case of the $\langle \epsilon_{yy} \rangle$ component (along the CD of the folding board) was particularly investigated. A linear approximation was chosen for this strain: see the dashed line on the graph 6. It was assumed that the slope of this line gives us the variation of the curvature $\Delta\kappa_{CD}^{DIC}$ of the sample along this direction when the relative humidity

Table 5 Typical dimensions of the fibres of the mechanical and chemical pulps used to build the folding board layers

	Mechanical pulp	Chemical pulp
Length (mm)	0.40	1.20
Width d_{\max} (μm)	30	24
Thickness d_{\min} (μm)	25	10

Table 6 Variation of the curvature in the cross direction of the folding board sample for a relative humidity jump from 20 to 50% RH, measured macroscopically and assessed by DIC

$-\kappa_{CD}$ (m^{-1})	1.5
$\Delta\kappa_{CD}^{DIC}$ (m^{-1})	1.4

jumps from 20 to 50%. Results are presented in Table 6 where $-\kappa_{CD}$ can be interpreted as the variation of the macroscopic curvature when performing the same relative humidity jump. Both values are astonishingly close (6% of difference). From this point of view, these results may support the linear assumed strain variations of the components ε_{xx} , ε_{yy} and $2\varepsilon_{xy}$ of the discussed low order plate theories and tend to confirm that the imaged volume can be considered as representative. Of course, the presented results are not exhaustive and should be further confirmed but they appear as promising. However, it can be noticed that, as stated by [29], laminate models of folding boards should certainly account for the in-plane, shear and through-thickness strain components in order to be able to describe strain and stress fields and to predict for instance damage occurrence in these materials.

Conclusion

In view of preserving the paperboard integrity and optimizing the runnability during printing and converting operations, it is important to understand the main phenomena governing the hygroexpansive behaviour of folding boards. Thus, a study was performed at the macroscopic and mesoscopic scales using a DIC method. This technique was applied to 2D images extracted from a microtomographic volume subjected to relative humidity changes. The hygroexpansive behaviour was found largely anisotropic. The hygroexpansion is five to ten times greater in the thickness direction than in plane. This technique shows that the hygroexpansion of each layer of the folding board is highly dependent on its fibre content. The relative evolution of the volumes of the pore and fibre phases was shown to exhibit schematically two types of behaviours. For layers having high fibre content (or similarly high density), the fibre phase volume is increased with the moisture content and the pore phase volume is shown to follow the fibrous network expansion. For layers having low fibre content (or low density), the fibre phase volume highly increases with the moisture content but the pore phase volume decreases simultaneously. This effect compensates largely the fibrous network expansion. Such results are in accordance with previous assumptions of the hygroexpansion of freely and restrained dried papers by Salmén and Fellers [9]. The hygroexpansive behaviour

observed for the imaged volume is thought to be representative of the hygroexpansive behaviour of the studied paperboard. This is supported by the agreement of average hygroexpansion values measured by DIC with those obtained at the macroscopic scale. Moreover, theoretical considerations on the hygroexpansive behaviour of the fibre network tend to confirm this statement. These results allowed also a discussion of the usual models developed for curl predictions. Some modifications of these models could be proposed based on the DIC measurements. The proposed approach can be adopted for studying the hygroexpansion of various materials such as papers, boards, non-woven materials and composites containing wood fibres and more generally plant fibres. It should be noticed that this technique does not allow yet the measurement of the deformation of individual fibres of the fibrous network. To date, this represents a great challenge for fibrous media analysed by microtomography and will demand for the development of specific image analysis techniques.

Acknowledgements This study was performed within the framework of the ESRF Long Term Project (exp. MA127) “Heterogeneous Fibrous Materials”.

References

1. Stöckmann VE (1974) Tappi 57(10):108
2. Uesaka T (2002) Handbook of physical testing of paper, Chapter 3. Dimensional stability and environmental effects on paper properties. Marcel Dekker, Inc., New York, pp 115
3. Uesaka T, Moss C, Nanri Y (1992) J Pulp Paper Sci 18(1):11
4. Uesaka T (1994) J Mater Sci 29:2373. doi:10.1007/BF00363429
5. Salmén L, Boman R, Fellers C, Htun M (1987) Nord Pulp Paper Res 2(4):127
6. Nanri T, Uesaka T (1993) Tappi J 76(6):62
7. Gallay W (1973) Tappi 56(12):90
8. Salmén L, Fellers C, Htun M (1985) In: Fundamental Research Symposium, Oxford
9. Salmén L, Fellers C (1989) J Pulp Paper Sci 15(2):63
10. Carlsson L (1981) Fibre Sci Technol 14:201
11. Lif J, Fellers C, Sjöremark C, Sjöödahl M (1995) J Pulp Paper Sci 21(9):302
12. Rolland du Roscoat S, Thibault X, Bloch J-F (2005) J Phys D Appl Phys 38:A78
13. Rolland du Roscoat S, Decain M, Thibault X, Geindreau G, Bloch J-F (2007) Acta Mater 55:2841
14. Neagu R, Gamstedt E, Lindström M (2005) Composites A 36:772
15. Vacher P, Dumoulin S, Morestin F, Mguil-Touchal S (1999) Proc Inst Mech Eng C ImechE 213:811
16. Niskanen K (1998) Papermaking science and technology, book 16, paper physics. Fapet Oy, Helsinki
17. Paulapuro H (2000) Papermaking science and technology, book 1, stock preparation and wet end. Fapet Oy, Helsinki
18. Rolland du Roscoat S, Decain M, Geindreau C, Thibault X, Bloch J-F (2008) Appita J 61:286
19. Le Corre S, Dumont P, Orgéas L, Favier D (2005) J Rheol 49:1029
20. Toll S (1993) J Rheol 37:123
21. Batchelor WJ, He J, Sampson WW (2006) J Mater Sci 41:8377. doi:10.1007/s10853-006-0889-7

22. He J, Batchelor WJ, Johnston RE (2004) *Appita J* 57(4):292
23. Sampson W (2009) *Int Mater Rev* 54:134
24. Alava M, Niskanen K (2006) *Rep Prog Phys* 69:669
25. Schlecht M, Schulte K, Hyer MW (1995) *Compos Struct* 32:627
26. Gendron G, Dano M, Cloutier A (2004) *Compos Sci Technol* 64:619
27. Bortolin G, Gutman P, Nilsson B (2006) *J Process Contr* 16:419
28. Dano M-L, Bourque J-P (2009) *Int J Solids Struct* 46:1305
29. Reddy J (2000) *Mechanics of laminated composite plates and shells theory and analysis*. 2nd edn. CRC Press LCC publishing, Boca, Raton, FL, USA